Title	Suspended particulate matter concentration in response to tidal hydrodynamics in a long mesotidal floodway
Author(s)	Xiao, Cong; Kawanisi, Kiyosi; Al Sawaf, Mohamad Basel
Citation	Estuarine, Coastal and Shelf Science , 233 : 106525
Issue Date	2020-02-05
DOI	10.1016/j.ecss.2019.106525
Self DOI	
URL	https://ir.lib.hiroshima-u.ac.jp/00051056
Right	© 2020. This manuscript version is made available under the CC-BY-NC-ND 4.0 license http://creativecommons.org/licenses/by-nc-nd/4.0/ This is not the published version. Please cite only the published version. この論文は出版社版ではありません。引用の際には出版社版をご確認、ご利用ください。
Relation	

Suspended particulate matter concentration in response to tidal hydrodynamics in a long mesotidal floodway

Cong Xiao [a], Kiyosi Kawanisi [a*], Mohamad Basel Al Sawaf [a]

[a] Department of Civil and Environmental Engineering, Graduate school of Engineering, Hiroshima University, 1-4-1 Kagamiyama, Higashihiroshima, 739-8527, Japan

Abstract

Analyses of seasonal data obtained using acoustic Doppler current profilers provide an understanding of the behavior of suspended particulate matter concentration (SPMC) toward different forcings in tide-controlled floodways. In this work, the relative contributions of external forcings on SPMC variability were quantified in a tidal river system using singular spectrum analysis (SSA). The main environmental features affecting SPMC were identified as i) spring-neap tidal oscillation, ii) the ebb/flood velocities, and iii) tidal straining. Large SPMC fluctuations occurred under strong mixing states and were directly related to the sediment resuspension stirred up by spring-neap tidal cycles (73.6%–81.9%) and ebb/flood velocities (9.6%–19.5%). On the seasonal scale, river discharge is the key variable explaining the downstream flushing and promoting the occurrence of a

*Corresponding author.
E-mail address: kiyosi@hiroshima-u.ac.jp (K. Kawanisi)

convergence zone at the floodway. Upstream from the floodway (greater than 4.8 km from the river mouth), the spring-neap tidal oscillation dominated the suspended particulate matter (SPM) mobility under low river discharge. Two interesting findings were revealed in this work: (i) the SPMC/SPM transport variation responses to tidal forcing (tidal asymmetry) were dominated and modified by river discharge and (ii) the effect of river discharge on the SPMC/SPM transport did not result in a uniform state along the floodway. It is believed that these findings provide further understanding of the dynamics of suspended sediments in shallow tidal systems.

Keywords: Acoustic Doppler current profiling, tidal hydrodynamics, suspended particulate matter, estuary, single spectrum analysis, spring-neap tidal oscillation

1. Introduction

The dynamics of suspended particulate matter (SPM) are intricate in estuarine systems and significantly vary with time and spatial scale. The distribution of SPM in a water column results from the combined processes of erosion, deposition, and transport. Moreover, the suspended particulate matter concentration (SPMC) is modified by the overall variations of multiple controlling factors (Murphy and Voulgaris, 2006). Hence, additional comprehensive investigations and analyses of these factors and their interactions during different specific time scales are vital for understanding the transport mechanisms of SPM.

Environmental forcings related to SPMC in estuarine environments have been well investigated (Kaneko et al., 1997; Zhu et al., 2000; Ferreira et al., 2003; Baeye et al., 2011). Forcings can be divided into two main categories: (1) deterministic (tidal cycle, tidal range) (Voulgaris and Meyers, 2004) and (2) stochastic (runoff, wind) constituents (Baeye et al., 2011). These categories are characterized by multiscale, unstable, and nonlinear dynamic processes. Hence, quantifying the contributions of different driving factors to SPMC variability is a difficult task that has barely been studied. Schoellhamer (2002) and French et al. (2008) applied the singular spectrum analysis (SSA) method to quantify the suspended sediment concentration variability related to environmental forcings in San Francisco Bay and Blyth Estuary, respectively. The SSA method was applied to high-frequency time-series data, however, these studies were restricted to single cross-sections of the systems and lacked a detailed analysis of seasonal differences of controlled forcings.

To analyze sediment transport dynamics and the spatiotemporal variability of the responses of suspended particles to tidal hydrodynamics thoroughly, prior information about the SPMC is essential. However, it is difficult to measure these rapid fluctuating characteristics in riverine environments. Traditional techniques for laboratory analysis of SPMC often rely on periodic *in-situ* water sampling (Murphy and Voulgaris, 2006). Expectedly, these approaches may be satisfactory for many applications but still have limitations, especially in estuaries, owing to uncertain characteristics of suspended particles. However, gathering water samples may be not sufficient to characterize the behavior of suspended particles over a long time, due to the variations in the transport of suspended materials brought by changes in tidal velocity, tidal range, and wind effects.

In large-scale studies, acoustic Doppler current profilers (ADCP) have been used for decades to measure currents. In recent years, the amplitudes of back-scattered signals have been used to detect the SPMC (Moore et al., 2013; Latosinski et al., 2014). Furthermore, there have been recent studies on measuring suspended sediments by using swath bathymetry systems (Duncker et al., 2015). In smaller-scale studies, noteworthy, advanced efforts have been made through the use of sound backscatter to study near-bed sediment transport processes (Moura et al., 2011). Acoustic profilers are being developed for near-bed studies and can estimate both suspended sediment concentrations and current profiles with high spatial–temporal resolutions and provide necessary information about bedform variations.

Estuarine systems have several problems associated with maintenance with respect to factors such as dredging, port development, and regulation of incoming river flow. For example, in the case of the Yangtze river, the annual discharge is 2.93×10^4 m^3/s, and the annual mean suspended sediment load is 4.9×10^8 tons (Shi, 2010). Tidal currents and tidal asymmetry play important roles in sediment mobility; however, sediment mobility is directly related to discharge. In the case of Otagawa estuary, Hiroshima, Japan, tidal hydrodynamics primarily determine the fate of suspended sediment in the case of limited runoff (Kawanisi and Yokosi, 1997; Razaz and Kawanisi, 2012). As an example, in the Rotterdam Waterway estuary, nearly 75% of the fine sediment is imported from the sea by tides (Van Leussen and Dronkers, 1988).

In this study, we aimed to reveal sediment dynamics under tidal hydrodynamics with low river discharge. Several fundamental issues related to tidal hydrodynamics remain unanswered, such as the main factors that contribute to sediment exchange processes between the bed and overlying water. Therefore, tracing these variations temporally and geographically is important to achieve a clear understanding of sediment dynamics, and knowledge of sediment dynamics can facilitate the management of estuarine systems. The main purpose of this study was to quantify the effects of tidal forcings on the SPMC variability in a tide-controlled channel, in order to shed light on SPMC dynamics in response to tidal hydrodynamics. The remainder of this paper is structured as follows. The descriptions of the study area and methods for data processing are given in Section 2. The results and discussion are provided in Sections 3 and 4, respectively. Finally, the conclusions are presented in Section 5.

2. Materials and methods

2.1 Study area

The Otagawa estuary is composed of a shallow and tide-controlled delta with several channels. The maximal tidal compartment range reaches up to around 13 km from the river mouth (Razaz et al., 2015). The Ota river divides into two main branches nearly 9 km upstream from the river mouth. Rows of Gion sluice gates control the volume of the runoff. In the case of normal operation, two gates are closed and only one gate is slightly opened to release water with a controlled cross-section of

32 m×0.3 m. During flood events (when the discharge at Yaguchi station is greater than 400 m^3/s), all of the sluice gates are completely opened and the freshwater runoff from the Gion sluice gates is designed to be about half of the total river discharge. The geometry of the sluice gates and the accumulated sediment around the gates along with asymmetric tidal currents produce an unstable and complicated flow system. The flow pattern varies considerably with both the tidal phase and the amount of runoff flowing through the gates.

Razaz et al. (2015) pointed out that tidal straining and bathymetry are the main sources of flocculation in the Otagawa floodway. Kawanisi et al. (2008a) discussed the effects of river discharge, tidal range, and wind on the transport of sediment. They revealed that there was suspended sediment transport upstream within the spring tide. The upstream transport increased with increasing tidal range and decreased with increasing distance from the mouth. At the flood events, the suspended sediment was transported downstream. A long-term discharge monitoring campaign was conducted using the fluvial acoustic tomography (FAT) system, showing that around 20% of the total Ota River discharge flowed into the floodway on normal days and that it received up to 50% of the total runoff during flood events (Kawanisi et al., 2010). Furthermore, it was reported that the maximum tidal current velocities during flood and ebb were around 0.65 m/s and 0.5 m/s, respectively, and during the spring tide the peak tidal range reached 4 m at the river mouth (Razaz et al., 2015). In general, due to the limited runoff under normal conditions and mesotidal inflow from Hiroshima Bay, the estuarine circulation in the Otagawa floodway is moderate.

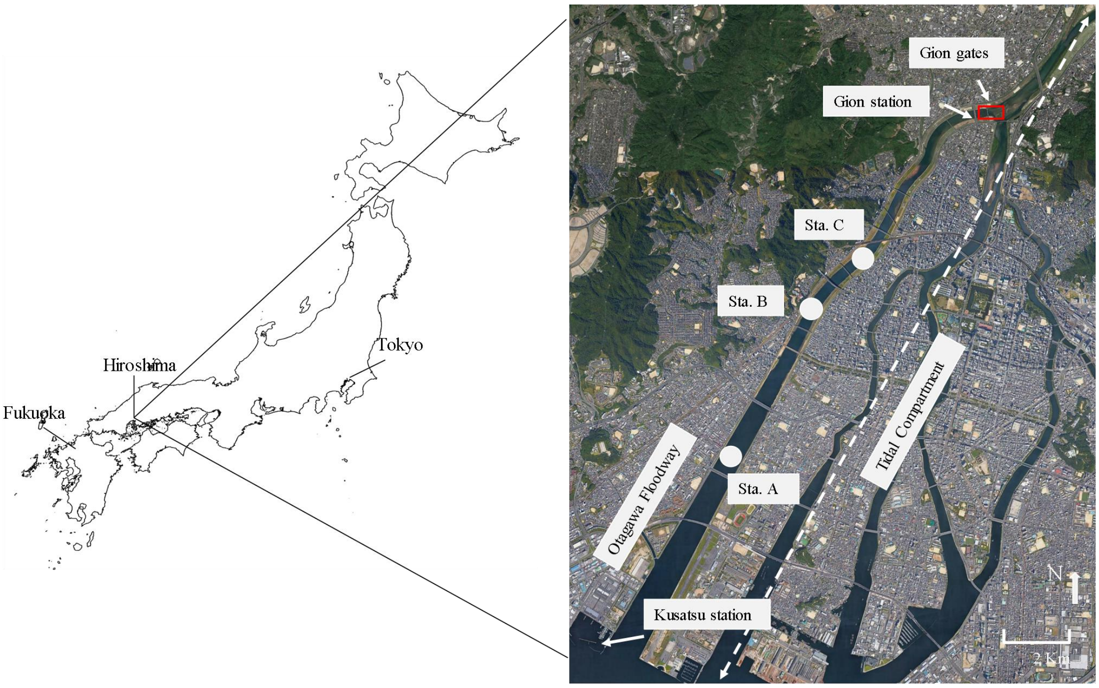

Fig. 1 Research area and observation sites along the Otagawa floodway, Hiroshima City, Japan.

2.2 Instruments and methods

Three locations along the floodway in the Ota estuary were selected as observation sites. Stations A, B, and C were located 2.8 km, 4.8 km, and 6.0 km upstream from the river mouth, respectively, as illustrated in Fig. 1. Several field observations were performed on the Otagawa floodway at different periods. At station A, measurements of hydrodynamics and sediment variables were performed during two periods: from July 29 to August 16, 2007 and from January 6 to 27, 2008. During the observation periods, a 2 MHz ADCP (Aquadopp Profiler, Nortek) was installed to measure the 3D velocities and backscatter intensity in the water column, with a 20 min sampling interval and average interval of 180 s. The bin size was set as 0.1 m, the bin number was 55, and the blank distance was 0.05 m. During summer, the ADCP was installed about 30 m away from the right bank (simply expressed as Sta. A_R) and it was set upward in the water column. During winter, the ADCP was installed at the center of the channel (simply expressed as Sta. A_C) and it was set downward from the water surface. During both field observations, a conductivity–temperature–depth sensor (Compact-CTD, JFE Advantech) was set around 0.4 m above the river bed to collect depth, salinity, temperature, turbidity, and chlorophyll-a data every 20 min during each observation period to identify the basic features of the estuary. At stations B and C, the ADCP sampling strategies were the same as those at station A. The observations at stations B and C were performed from December 22, 2007 to January 16, 2008 and from December 27, 2007 to January 10, 2008, respectively. In-situ water samples were suctioned during the observation period for ADCP backscatter calibration. Eight samples for particle size analysis were also collected, on December 12, 2007. The sample sites were located 0.5, 1.5, 2.5, 2.8, 3.5, 4.9, 7.0, and 8.0 km upstream from the mouth.

The SPM acoustic model of scattering has been employed by different researchers (Thorne and Hanes, 2002). In this work, the basic SPM modeling equations were used to calculate the concentration. For further details on this SPM acoustic model, readers can refer to Kawanisi et al. (2008b), Latosinski et al. (2014), etc. The relationship between the acoustical backscatter intensity of ADCP and the water sample concentration was established, and the obtained coefficients of regression R^2 were 0.70, 0.69, and 0.65 at Stations A, B and C, respectively. Moura et al. (2011) discussed the observation of SPM using different acoustic instruments in a shallow estuarine system with a low SPMC, reporting that the coefficients varied from 0.6 to 0.9. In this study, the validation results are appropriate for use in SPMC variation analysis.

SSA is similar to principal component analysis (Schoellhamer, 1996). This method is capable of extracting the necessary information related to environmental parameters from short/long time series data without previous knowledge of the nonlinear hydrodynamics (Schoellhamer, 2001). The SSA method is based on the concept of sliding a window of width *M* down a time series to obtain an autocorrelation matrix (Vautard et al., 1992). Then, eigenvectors (empirical orthogonal functions) and eigenvalues (*k*) of the lagged autocorrelation matrix are calculated. Afterwards, the random raw series data can be decomposed into several simpler periodic time series spectra, i.e., the so-called reconstructed components (RCs). The RCs are calculated by multiplying eigenvectors times their corresponding principal components. Each contribution per variance is presented in terms of its eigenvalues *k*. Most of the variability is contained in the first RCs, and the remaining RCs consist of noise signals. For further details, readers can refer to Jalón‐Rojas et al. (2016)

3. Results

3.1 Hydrodynamic characteristics in the Otagawa floodway

The seasonal differences in river discharge, water depth, salinity, water temperature, and current velocity profiles during summer from July 29 to August 16 (Sta. A_R) and during winter from January 6 to 26 (Sta. A_C) are shown in Figs. 2 and 3, respectively. In summer, the compact-CTD was deployed two times, firstly from July 29 to August 2 and then from August 10 to 16. In this work, we did not compare the variations between the water discharge approaches (i.e. FATS and the Rating Curves method). In fact, there exist some differences between the two discharge methods (i.e. FATS and Rating Curves) in the short term (a few hours). Nonetheless, it was demonstrated that the low-frequency variations of water discharge were similar (Kawanisi et al., 2016; Al Sawaf et al., 2017). In this study, the discharge from Gion gates was not available. Razaz (2010) showed the relationship between the discharge from Gion gates (Q_{Gion}) and Yaguchi ($Q_{Yaguchi}$) station, and in this research we referred to this relationship to convert $Q_{Yaguchi}$ into Q_{Gion} for further assessment. Hence, in the related figures, the main labels are shown and marked according to the discharge values recorded at Yaguchi station. In summer, the water discharge ($Q_{Yaguchi}$) was higher, with maximum values up to 400 m^3/s (Q_{Gion} = 242 m^3/s) (Fig. 2a). In contrast, during winter, the maximum discharge ($Q_{Yaguchi}$) was around 130 m^3/s (Q_{Gion} = 27 m^3/s) (Fig. 3a). Moreover, a clear sign of tidal excursion is visible in the water depth time series across the surveyed periods. Owing to the saltwater intrusion from Hiroshima Bay, the water has higher salinity at deeper levels. The water is warmer at deeper levels during winter, while during summer, the lower water is colder than the upper water. During low water depth, intermittent variations of salinity and temperature were occurred as a result of tidal straining, as revealed in Figs. 2c, 2d, 3c, and 3d. Field data from summer and winter revealed the reciprocating tidal current in the floodway and indicated a strong flood-ebb tidal cycle (Figs. 2e and 3e). Apparently, the ebb current was greater than the flood velocity during neap tide, whereas the vertical velocity gradients during spring tide were minimal. In general, the hydrodynamics of the Otagawa floodway are dominated by spring-neap and flood-ebb tidal cycles. Moreover, the hydrodynamics are modified by the river runoff.

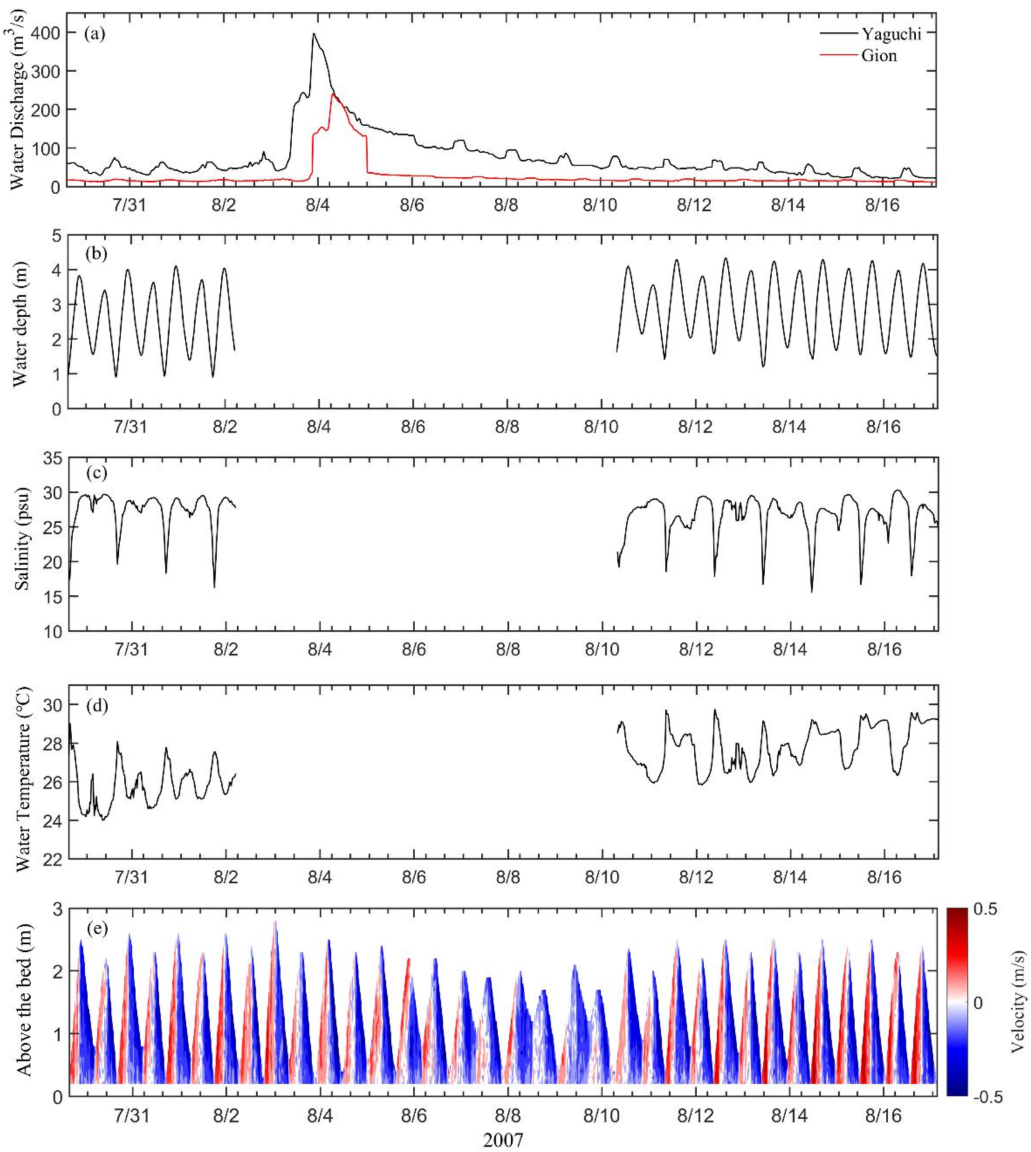

Fig. 2 Hydrodynamic data during summer at Sta. A_R from July 29 to August 16, 2007.

Temporal variations in (a) river discharge at Yaguchi gauging station, (b) water depth, (c) salinity, (d) water temperature, and (e) velocity. The red and blue values indicate the flood and ebb velocities, respectively. The compact-CTD was deployed two times, firstly from July 29 to August 2 and then from August 10 to 16. The Yaguchi gauging station is located around 14.6 km from the river mouth (not shown in Fig. 1).

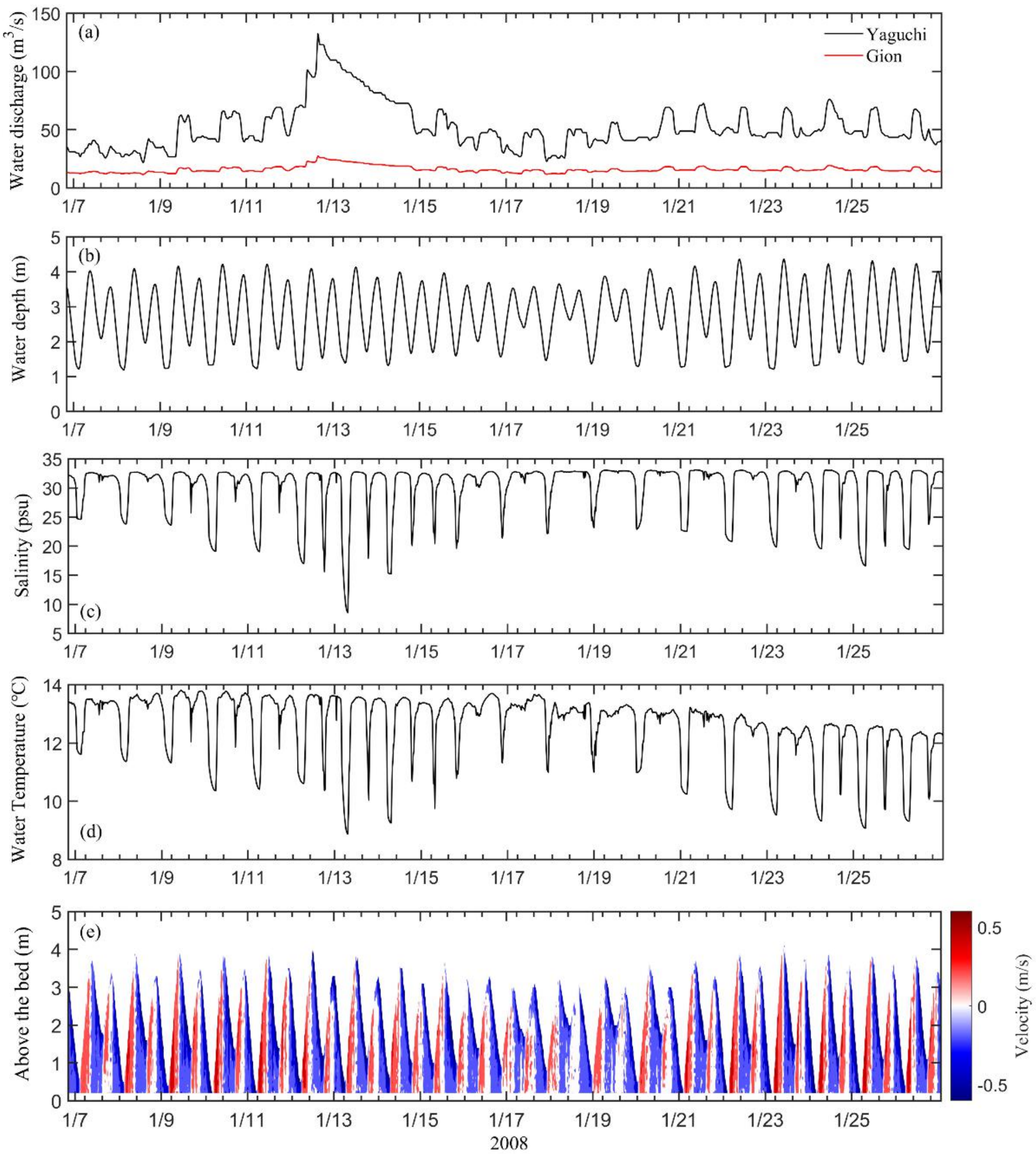

Fig. 3 Hydrodynamic data during winter at Sta. A_C from January 6 to 26, 2008. Temporal variations in (a) river discharge at Yaguchi gauging station, (b) water depth, (c) salinity, (d)

water temperature, and (e) velocity. The red and blue values indicate the flood and ebb velocities, respectively. The Yaguchi gauging station is located around 14.6 km from the river mouth (not shown in Fig. 1).

3.2 In-situ suspended particulate matter concentration variations and sediment size distributions

During the observation periods, the SPMC time series were estimated from the ADCP backscatter. Hydrodynamic parameters that provide information about the variations of particles enable us to understand the mechanisms that may control the changes in SPMC during summer and winter and at different locations (spatiotemporal variations). The temporal variations in the depth-averaged SPMC are shown in Fig. 4. During summer, the SPMC at Sta. A_R ranges from 0.5 to 100 mg/L and responds significantly to spring-neap tidal fluctuations (Fig. 4a). In winter, the SPMC variability at Stations B and C is characterized by a local maximum and a minimum, ranging from 0.01 to 50 mg/L and corresponding to the spring and neap tides (Figs. 4c and 4d). Meanwhile, the intermediate SPMC at Sta. A_C (Fig. 4b) is about one order of magnitude larger than those at Stations B and C, with the maximum values up to 90 mg/L during the spring tide. Higher SPMC values are observable at Sta. A_C, relatively lower SPMCs appear at Sta. B, and the SPMC at Sta. C is the lowest. Generally, the qualitative variation in the SPMC is very similar to the tidal cycle pattern, which indicates the influence of tidal flow. As shown in Figs. 2a and 3a, significant increases in river discharge can be observed around August 4 and January 12. Meanwhile, a higher SPMC can be captured, although not during the spring tide periods. The higher SPMC can be attributed to the influence of river runoff. Usually, SPMC fluctuations are well related to the spring-neap tidal cycle, i.e., to the higher tidal range that occurs during the spring tide. Although the spring tide is based on the lunar age, it does not entirely match the maximum tidal range. The SPMC is greater when the tidal range is maximal.

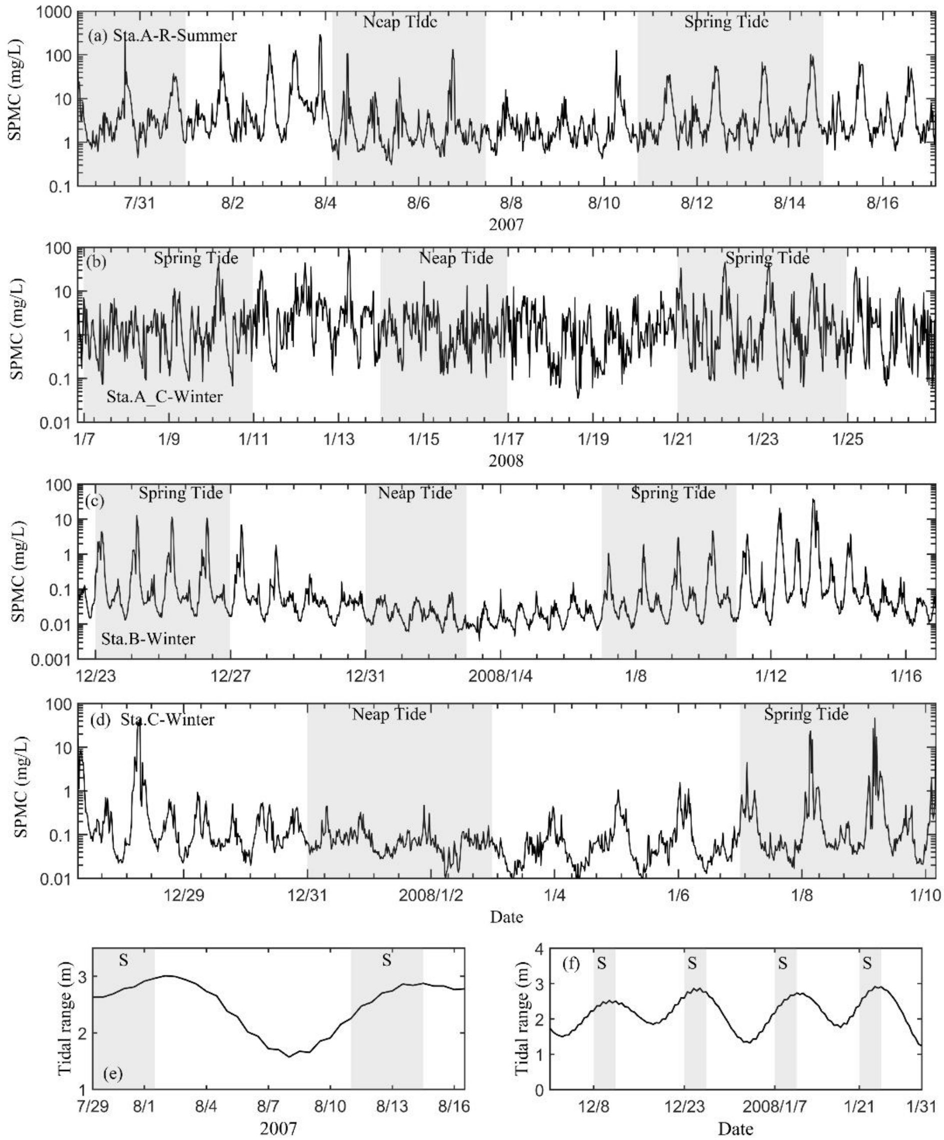

Fig. 4 Depth-averaged SPMC time series along the Otagawa floodway: (a) during summer at

Sta. A_R from July 29 to August 16, 2007, (b) during winter at Sta. A_C from January 6 to 26, 2008, (c) during winter at Sta. B from December 22, 2007 to January 16, 2008, and (d) during winter at Sta. C from December 27, 2007 to January 10, 2008. Tidal range from Kusatsu gauging station during (e) summer and (f) winter. The shaded regions represent the spring/neap periods.

For further clarification, the grain size distributions in the study area were examined from eight sites selected along the floodway from the river mouth to near the Gion sluice gates, as presented in Fig. A.1. The bed materials in the Otagawa floodway, where the bed slope is about 1/3300, mainly consist of sand containing a little silt and clay. The grain size distribution varies from upstream to the river mouth. The proportion of small particles increases closer to the river mouth. The particle size distributions can be divided into two types: (1) Type I, where the distance from the mouth is less than 3.5 km and the slope of the curve is the steepest when the volume percentage is less than 80%, which means that there are more fine particles; and (2) Type II, where the distance is greater than 3.5 km and the curve has a flatter slope when the volume percentage is less than 20%, which means that there are coarser particles, which are more difficult to resuspend in the water column.

3.3 SSA results and fast Fourier transform (FFT) test

3.3.1 SSA results

As above stated, the SPMC varies remarkably in response to tides and streamflow. Unfortunately, these factors induce SPMC variability at comparable orders of magnitude and descriptive methods are not sufficient to compare their relative effects at different time scales. Compared to a qualitative interpretation, SSA is more rigorous approach for illustrating all temporal characteristics of SPMC variability and the corresponding environmental factors. SSA can be utilized not only to characterize SPMC variability, but also to determine the relative contributions of influencing factors to the total variation.

Before applying SSA, the SPMC time series was smoothly filtered with a 1 h moving average to remove noise. There exists a small difference between the raw and filtered data. The R^2 values and root mean square errors (RMSEs) of four SPMC series of data ranged between 0.76 and 0.97 and between 0.10 and 0.27 mg/L, respectively. The SPMC data were decomposed into 10 modes by SSA (RCs, Fig. A.2a). SSA was applied to the SPMC time-series data with a window size of 24 h. Once evaluated, each RC group was assigned to one or two control forcing frequencies.

At Stations B and C, RC1 contribute 96.9% and 94.5% of the data, respectively. The contributions of other modes to the SPMC variation are negligible. At Sta. A_R in summer, RC1 contributes 81.9% and RC2 accounts for 9.6% of the data, while in winter at Sta. A_C, RC1 and RC2 account for 73.6% and 19.5%, respectively. Thus, in the following discussion, we focus on analysis of the first RC at Stations B and C, and the first two RCs at Sta. A_R and Sta. A_C.

During summer, at Sta. A_R, RC1 accounts for 81.9% of the data, where the oscillations are similar in amplitude to the tidal velocity, and the positive RC1 values responded to the significant spring-neap tidal cycle (Fig. 5a). RC2 accounts for 9.6% of the variation and varies negatively with the water depth and positively with the tidal current velocity (Figs. 5b, 5c, 5e, and 5f), indicating the influence of the tidal velocity. According to this interpretation, it can be assumed that RC1 contains the variance of the spring-neap tidal cycle and RC2 contains the intra-tidal modification of the semidiurnal tide. Like the situation in summer, in winter at Sta. A_C, the first RC contributes 73.6% of the variation and varies positively with the spring-neap tidal cycle (Fig. 6a), indicating the controlling role of the spring-neap tidal cycle. RC2 explains 19.5% of the variations that vary negatively with the water depth and positively with the tidal velocity (Figs. 6b, 6c, 6e, and 6f).

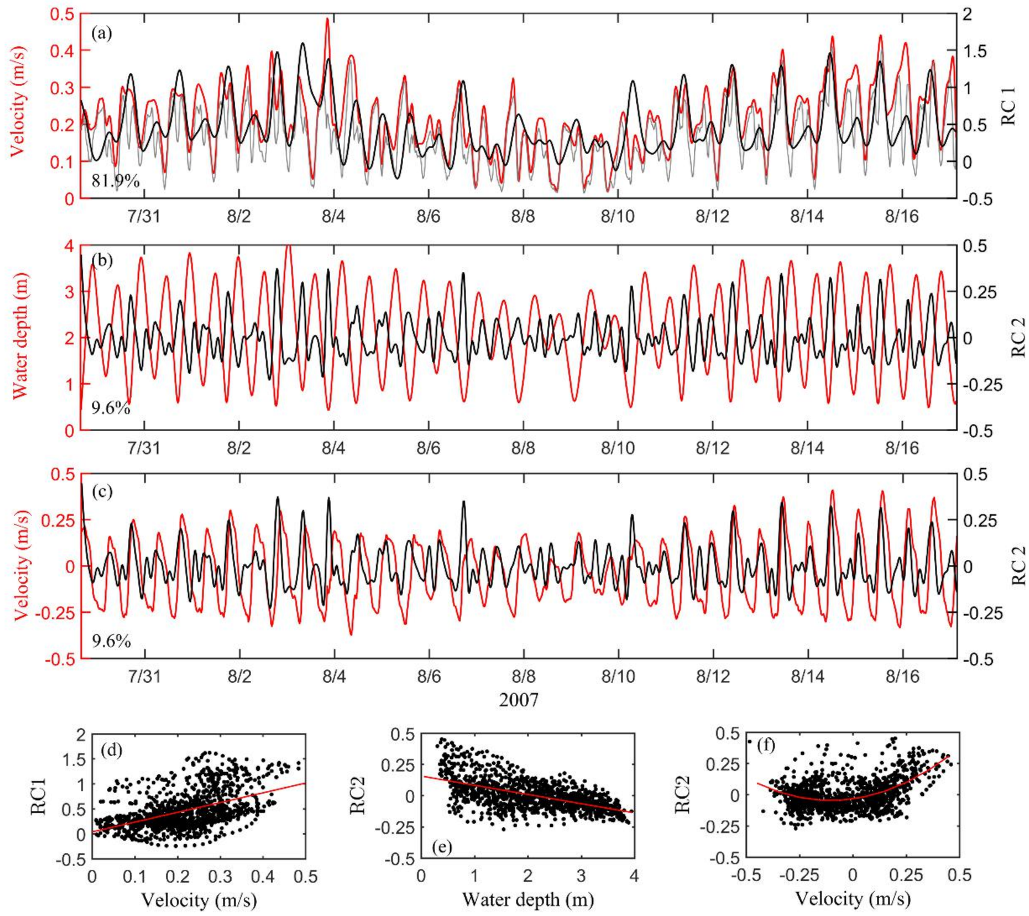

Fig. 5 Comparisons of RCs to the temporal changes of the variables at Sta. A_R: (a) RC1 vs. velocity (the red line represents the envelope of the velocity and the gray line represents the original magnitude of the velocity), (b) RC2 vs. water depth, (c) RC2 vs. velocity, (d) regression diagram of RC1 and velocity amplitude, (e) regression diagram of RC2 and water depth, and (f) regression diagram of RC2 and velocity. The contribution of each RC to the total SPMC variability is written in the bottom left corner, and these two modes contain 91.5% of the total variance.

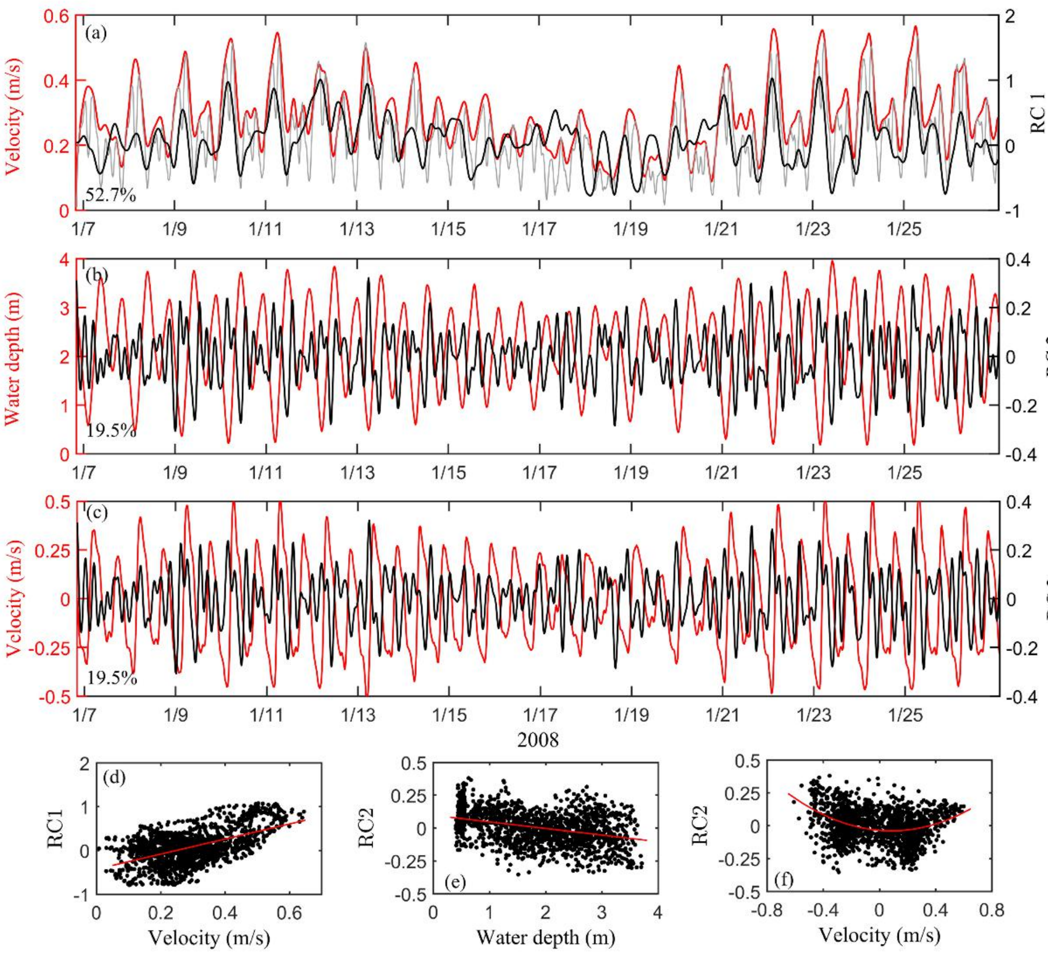

Fig. 6 Comparisons of RCs to the temporal changes of the variables at Sta. A_C: (a) RC1 vs. velocity (the red line represents the envelope of the velocity and the gray line represents the original magnitude of the velocity), (b) RC2 vs. water depth, (c) RC2 vs. velocity, (d)

regression diagram of RC1 and velocity amplitude, (e) regression diagram of RC2 and water depth, and (f) regression diagram of RC2 and velocity. The contribution of each RC to the total SPMC variability is written in the bottom left corner, and these two modes contain 93.1% of the total variance.

During winter, RC1 explains 96.9% and 94.5% of the variations at Stations B and C, respectively, and varies positively with the spring-neap tidal cycle (Fig. A.2b), indicating the strong influence of the spring-neap tidal cycle. Since this component primarily describes the fluctuations of the velocity amplitude, this component can be interpreted as the spring-neap tidal cycle caused by the variations in tidal velocity, and the water column is destabilized by the tidal velocities. Thus, the bottom sediment will be resuspended by the bed shear stress and reenter the water column due to vertical diffusion.

3.3.2 FFT test

Fig. 7 illustrates the FFT power spectra of the original SPMC time series on a log-log plot. It shows that the main variability has time scales of (a) 14 days, (b) 24 h, and (c) 12 h. These time scales are easily linked to deterministic forcings: spring-neap tidal fluctuations and ebb-flood tidal flow.

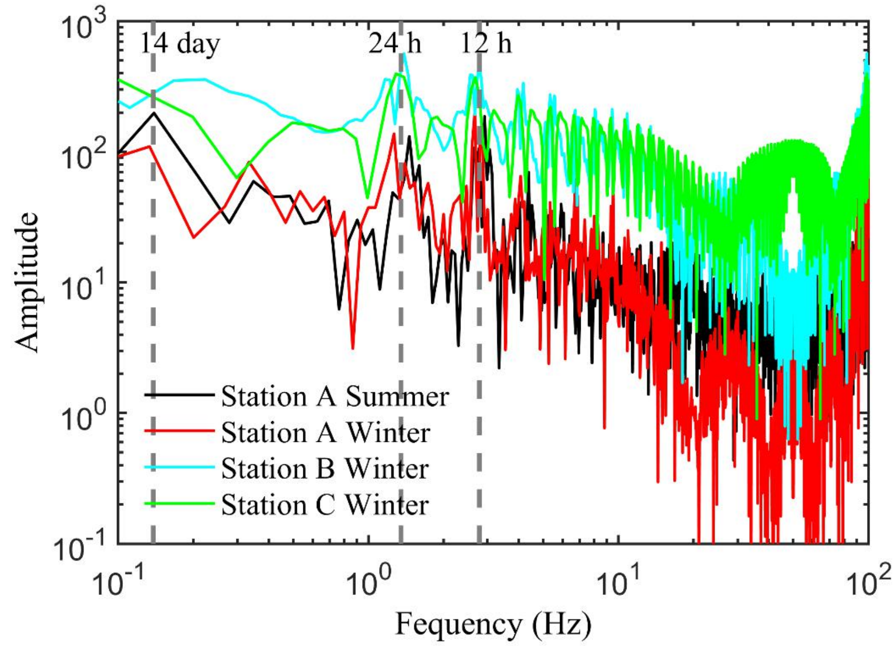

Fig. 7 FFT power spectra of the original depth-average SPMC time series.

In this study, the relative contributions of the driving forcings were investigated and their associated environmental forcings of the SPMC were demonstrated. The application of SSA and FFT confirmed the importance of tidal modulation on the SPMC during summer and winter. Additional information about these forcings will be comprehensively discussed later.

3.4 Spring-neap tidal cycle

The SPMC exhibits different variations during summer and winter, indicating the important role of tidal modulation. The Otagawa floodway is a tidally controlled estuarine system. The differences resulting from tidal mixing and stratification affect suspended sediment variations.

Commonly, the Simpson number is used as an indicator to demonstrate the intensity of tidal mixing (Burchard et al., 2011). The Simpson number is defined as the ratio of the potential energy change caused by tidal straining to the production rate of the turbulence kinetic energy (TKE). Therefore, the Simpson number is only useful in cases in which the horizontal gradients of the density and tidal velocity are known (Ge et al., 2018). Neglecting the effects of the horizontal density gradients, the growth rate of the bottom boundary layer can be parameterized similarly with the growth of a tidal velocity mixed layer. The following mixing indicator was proposed by Geyer and MacCready (2014) to count the efficiency of tidal mixing:

$$M^2=\frac{C_d U_T^2}{\omega N H^2}, \quad (1)$$

where C_d is the drag coefficient, U_T represents the amplitude of the tidal velocity, H is the water depth, ω is the tidal frequency, and

$$N=\sqrt{\frac{\beta g S_0}{H}}, \quad (2)$$

where N is the buoyancy frequency and S_0 is the reference salinity. In this work, the mean salinity during each observation period was adopted as S_0, g is the gravitational acceleration and was taken to have a constant value of 9.8 m/s^2. $\beta = (\rho/\rho_0 - 1)/s$ was used to estimate the instantaneous buoyancy frequency (Ge et al., 2018), where ρ is the instantaneous density, s is the instantaneous salinity, and ρ_0 is the reference density.

Applying these equations, the M values during summer and winter were calculated. Four major harmonic constants of the water level are shown in the Table 1. The water level data were obtained from the Kusatsu gauging station during the observation period. The M_2 tide dominated in the Otagawa floodway; thus, the estimated value of M was utilized for the M_2 tidal frequency. C_d was taken to be 0.0025 (Ge et al., 2018).

Table 1 Harmonic analysis of water level

Tides	Amplitude (m)	Phase (°)
M_2	1.02	272.11
K_1	0.34	226.29
O_1	0.26	190.09
S_2	0.34	322.88

For brevity, the intra-tidal variations on the velocity and SPMC at Station A are narrated in detail, while the behaviors of the tidal current and SPMC at Stations B and C are only stated briefly.

3.4.1 Summer

During the spring tide, the velocity profiles at Sta. A_R indicate the robust dominance of the semidiurnal tide. The ebb/flood velocities decrease from the surface to the bottom in the water column, and the tidal range is around 3 m (Fig. 4e), indicating a mesotidal environment. During the flood phase, the velocities are directed upstream with maximum values reaching 0.5 m/s; in the ebb, the velocities are directed downstream with maximum values around 0.55 m/s (Fig. 8a). The mean flood and ebb velocity durations are around 4.8 h and 7.2 h, respectively, with a 2.4 h difference in the water column. The ebb velocity and duration are greater than those during the flood tide, and the asymmetry can be attributed to the river runoff. Throughout our observations, the peaks of the bottom SPMC correspond to the peaks of the flood velocities just after the lower low water. In addition, the SPMC peaks match the peaks of *M* (Figs. 8b and 8c). Thus, the SPMC fluctuations are enhanced by increased flood velocities and likely by the local resuspension of SPM in the water column.

During the neap tide, the tidal range at Sta. A_R decreased to around 2 m (Fig. 4e). Compared to the maximum flood velocity during spring tide, the maximum flood velocity during neap tide (roughly 0.45 m/s) decreased by around 0.1 m/s. Meanwhile, the maximum ebb velocity was 0.55 m/s, which is almost equal to that during spring tide (Fig. 8d). The mean flood (around 3.6 h) and ebb (around 7 h) durations exhibit a larger difference, indicating a larger tidal asymmetry. This larger asymmetry reveals the role of river discharge in summer and the weak tidal variation during neap tide. The SPMC peaks occur together with the dominant ebb velocities during the lower low water, possibly due to the river discharge transport (Figs. 8d and 8e). In contrast to the spring tide, the local resuspension induced by flood currents decreases and most of the sediments stay near the bottom during the neap tide.

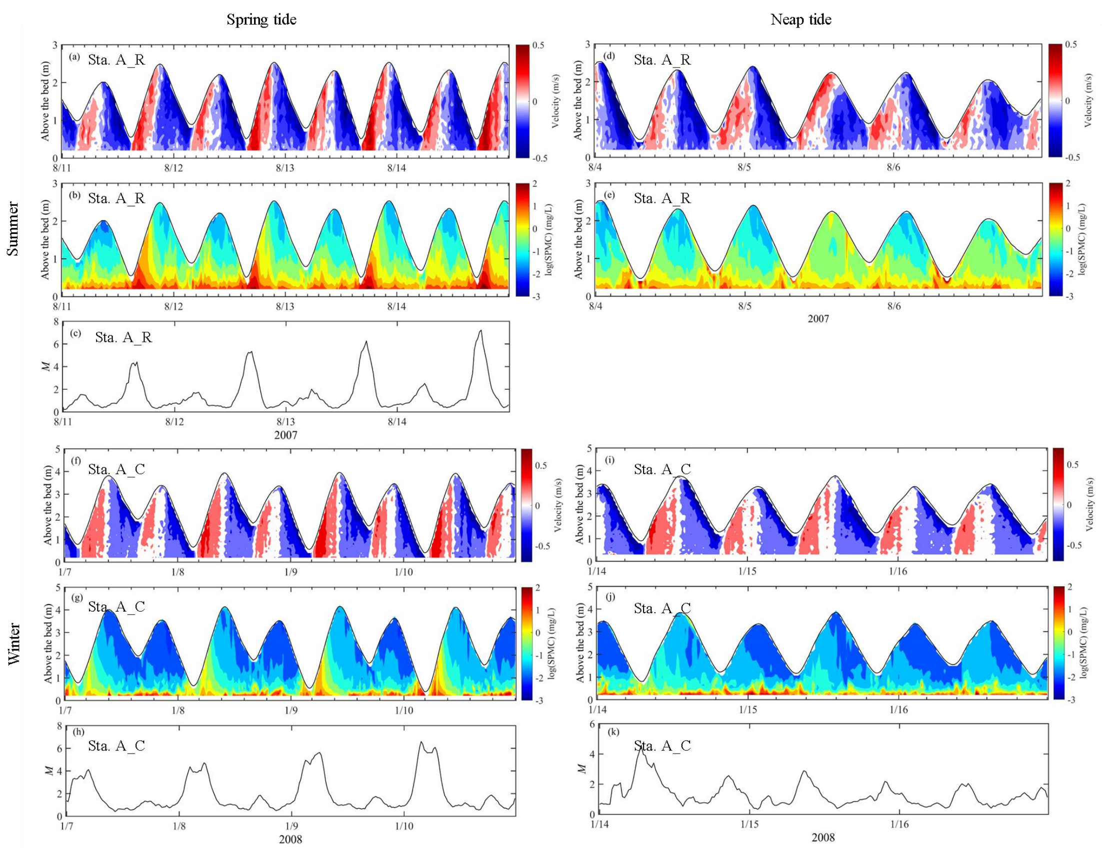

Fig. 8 Temporal variations of the velocity profiles (positive indicates flood, upstream), SPMC, and *M* at Sta. A_R in summer and Sta. A_C in winter during spring and neap tide. (a) Velocity, (b) SPMC, and (c) *M* during spring tide at Sta. A_R. (d) Velocity and (e) SPMC during neap tide at Sta. A_R. (f) Velocity, (g) SPMC, and (h) *M* during spring tide at Sta. A_C. (i) Velocity, (j) SPMC, and (k) *M* during neap tide at Sta. A_C.

3.4.2 Winter

The time series of the velocity, SPMC, and *M* over the spring and neap cycles during winter at Sta. A_C are shown in Fig. 8. During the spring period, the velocity decreases from the surface to the bottom, with the maximum flood and ebb velocities of up to 0.5 m/s and 0.55 m/s respectively (Fig. 8f). The vertically averaged flood and ebb durations at Sta. A_C during winter were around 4.8 h and 7.2 h, respectively. The SPMC peaks occur in the lower low water with the peaks in *M* and the flood velocity (Figs. 8g and 8h). During the neap tide, the low value of *M* at Sta. A_C indicates weaker tidal forcing conditions (Fig. 8k). The maximum flood/ebb velocities occur at the water surface, while most of the high SPMC values are near the bed (Figs. 8i and 8j). The peak of *M* corresponds with the larger SPMC that appears around the lower low water, and with larger flood and ebb velocities simultaneously. It can therefore be considered that the increased tidal velocity turbulence caused a local resuspension of sediments in the water column.

The variations of the SPMCs and current velocities at Stations B and C during the spring and neap periods in winter are similar to those at Sta. A_C (Fig. A.3). During the neap period, high SPMCs are observable closer to the bed, and the SPMC peak occurs just after the low water. Meanwhile, during the spring tide, significant SPMC fluctuations occur just after the lower low water, together with the increased flood velocities.

The SPMC at all stations fluctuates with the ebb/flood velocities. The SPMCs are higher at the peaks of the flood and ebb tidal flows, indicating the dominance of local resuspension on the SPMC variations. The spring tides match the occurrence of higher SPMC, whereas neap tides correspond to times of lower SPMC. This behavior is a result of higher tidal velocities during spring tides, which increases the availability of SPM within the brackish water column.

3.5 Relationship between SPMC and water discharge

Owing to the complex interactions between the tidal hydrodynamics, erodibility, and sedimentation, it is difficult to capture the essential information for the study of the role of tidal velocity and water discharge from Gion gates. Hence, to describe and capture the differences in the tidal transport of suspended sediments in the water column, the water column was divided into three vertical layers with similar thicknesses according to the instantaneous cell numbers of ADCP data. The average values (velocity and SPMC) within each layer (bottom, middle, and surface) were used to calculate the SPM transport.

In most cases, the river runoff is limited by the Gion sluice gates. During summer, well-mixed conditions are observable at spring tide for low river discharge $Q_{Yaguchi}$ < 110 m^3/s (Q_{Gion} < 24 m^3/s) (Figs. 2 and 8c). As depicted in Fig. 9a, the vertical SPMC distribution is scattered considerably during low discharge ($Q_{Yaguchi}$ < 110 m^3/s) and moderately during mid-flows (110 < $Q_{Yaguchi}$ < 250 m^3/s). Meanwhile, it is obvious that the SPMC varies smoothly during significant discharge periods ($Q_{Yaguchi}$ > 310 m^3/s). During winter, most of water discharge ($Q_{Yaguchi}$) is lower than 110 m^3/s (Q_{Gion} < 24 m^3/s) (Figs. 9b–9d). For each station, the SPMC and discharge are weakly correlated, and the SPMC has many comparable values within each layer.

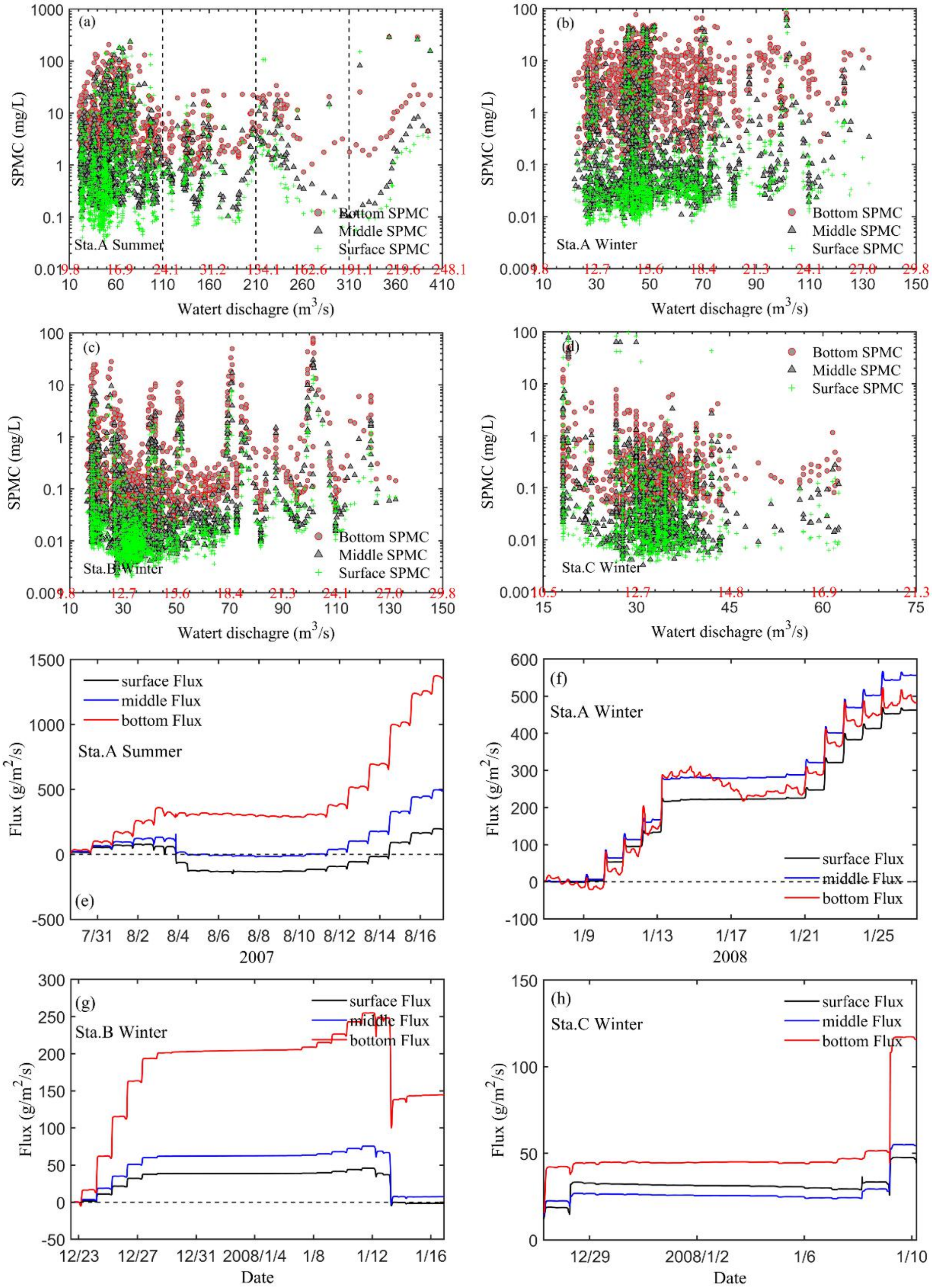

Fig. 9 (a)–(d) Scatter diagrams of SPMC and water discharge within three layers; (e)–(h) SPMC cumulative flux in three layers: (a) and (e) during summer at Sta. A_R from July 29 to August 16, 2007; (b) and (f) during winter at Sta. A_C from January 6 to 26, 2008; (c) and (g) during winter at Station B from December 22, 2007 to January 16, 2008; (d) and (h) during winter at Station C from December 27, 2007 to January 10, 2008 (positive: upstream direction, landward; negative: downstream direction, seaward).

During winter, in the case of low river discharge, Stations A, B, and C were mostly under the influence of tidal asymmetry. Tidal asymmetry causes flood velocities to be slightly dominant, and more sediments are resuspended, promoting significant upstream transport. Tidal transport at the three sites is directed upstream with magnitudes decreasing in the order of A > B > C, indicating that the sediment migration resulting from tidal hydrodynamics decreases from downstream to upstream (Figs. 9f–9h). In contrast, during summer, significant water discharge is evident from August 4 to 6, and the role of water discharge transport is highlighted (Fig. 9e). Seaward currents dominate during most of the tide, and the massive seaward transport of sand is produced during flood events. The significant feature is that the increased water discharge exerts an effect on suspended sediment transport and shifts the suspended sediment seaward. During winter, upstream tidal pumping at Station A dominates in the water column (Fig. 10f). At Stations B and C, the bottom layer exhibits upstream tidal pumping during the flood tide, while in the middle and surface layers, due to the bed slope and tidal asymmetry of the flow, downstream tidal pumping exists and counteracts part of the upstream sediment flux during the ebb tide (Figs. 9g and 9h).

4. Discussion

4.1 Role of tidal velocity and water discharge

Within tidal rivers, the interplay of the bed shear-stress and particle dynamics is key to understanding the effects of fluvial and marine influences on sediment transport and morphological development. In this study, we depended on the previous works that addressed flow, tide, and particle dynamics in the Otagawa floodway (Razaz and Kawanisi, 2012; Razaz et al., 2015) to assess the potential effects considering the river flow and tidal velocity.

4.1.1 Low water discharge

Processes that determine suspended particle dynamics in estuaries are functions of the turbulence intensity and suspended sediment load. The Otagawa floodway is characterized by moderate energy, low sediment concentrations, and stochastic events. The flocculation and resuspension of sediments are basically dominated by the processes associated with tidally induced shear stress followed by TKE production and dissipation (Razaz et al., 2015). The particles showed different proportions between downstream and upstream (Fig. A.1). Suspended particles are related to tidally induced shear stress at any single location, but the suspended sediment load shows a strong dependence on local sediment availability. Accordingly, the lower reach is supposed to experience more erosion and the upper reach will experience deposition.

For the low river discharge conditions, during spring tide, the mixing indicator *M* (Fig. 8) shows that the mixing is enhanced, with increased tidal range and velocities, and stratification is reduced. Our observations indicate that during these periods, the SPM at the lower and middle floodway is largely controlled by cyclical processes (resuspension, deposition, mixing, and upstream transport) driven by spring-neap fluctuations and ebb/flood velocities. At neap tide and low river flow, horizontal advection governs the SPMC (Razaz and Kawanisi, 2009). Uncles et al. (2002) indicated that the gravitational circulation at the lower estuary acts to concentrate the sediment at the estuary turbidity maximum (ETM), through an upstream flux of deeper suspended material. In this study, significant tidal asymmetries evidenced the importance of tidal pumping for SPM transport. Typically, most of the suspended material deposits at slacks, and resuspension with flood velocities are limited at neap tide. Wang et al. (2019) reported that water-sediment regulation schemes can change the tidal asymmetry and sediment transport. After the construction of channel regulation mechanisms in the Changjiang Estuary, the high-SSC area was enlarged and moved offshore. The Otagawa floodway acts as a freshwater regulation scheme, and the SPMC is well associated with tides. These processes promote sediment retention in the channel and reduce supply to the coast during the low-discharge season.

4.1.2 High water discharge

For high river discharge, significant tidal asymmetry in ebb/flood durations and velocities was observed (Fig. 2e). Scully and Friedrichs (2003) showed that a stronger tidal asymmetry on the ebb may act as a barrier that limits sediment suspension. This process may produce seaward pumping of suspended sediment (Fig. 9e). Ferreira et al. (2003) found that in the Guadiana River estuary, the ETM maintains its position for river discharge up to at least 250 m^3/s and suggested that the estuarine response to higher river discharge is buffered by the increasing stratification. In contrast, in the Tamar and Weser estuaries, Grabemann et al. (1997) showed that the ETM exhibited larger spatial variations and it is related to the variations with the river outflow. In light of the aforementioned ideas, it can be concluded that under high river discharge, flood currents were reduced, and freshwater inputs reinforced ebb currents (especially near the surface), causing the SPMC to increase rapidly. The observation results also indicated that when the river discharge ($Q_{Yaguchi}$) reached up to 400 m^3/s (Q_{Gion} = 242 m^3/s), the SPMC maximum was located at the lower reach and promoted a transient downstream transport (Fig. 9). The discharge from upstream and saltwater intrusion formed a two-layer structure with reduced vertical sediment diffusion and enhanced sediment-induced stratification.

4.1.3 Water circulation

Estuarine circulation is a major mechanism for tidal transport in partially mixed estuaries (Uncles et al., 2002). Following the classical theory of estuarine circulation, the bottom current is expected to flow landward in a salt wedge estuary due to the salinity gradient. The pressure gradient force $-\frac{1}{\rho_0}\frac{\partial p}{\partial x}$ is controlled by the combined effect of the seaward barotropic component $-g\frac{\partial\zeta}{\partial x}$ and the landward baroclinic component $-\frac{g}{\rho_0}\int_z^{\zeta}\frac{\partial\rho}{\partial x}dz$ that increase with depth. In the Otagawa floodway, with the lower river discharge $Q_{Yaguchi}$ < 110 m^3/s (Q_{Gion} < 24 m^3/s), the landward baroclinic term could suppress the seaward barotropic term. The tidal straining is critical in modifying the density structure at the saltwater wedge. Bottom water can overlap with the surface freshwater runoff via tidal straining and induced unidirectional upstream sediment transport during spring tide. On the other hand, for high river discharge $Q_{Yaguchi}$ > 310 m^3/s (Q_{Gion} > 191 m^3/s), saline water was flushed out from the upper reach. The stratification vanished around the low water and remarkable downstream transport was shown (Kawanisi et al., 2006), with the water regime transiently transitioning from tidally dominated to river dominated conditions. In the downstream region, the saltwater wedge still exited and could intrude through flood tides. The landward baroclinic term suppressed the seaward barotropic term; therefore, stratification existed around the high water.

4.2 Capture depocenter

Estuarine systems that have stronger flood currents than the ebb velocities (so-called tidal asymmetry) are more likely to accumulate sediments in their upper reaches. This characteristic is the result of enhanced resuspension and transport processes that occur during the flood tide period (so-called tidal pumping). Tidal oscillation effects are strong under low discharge conditions, with magnitudes decreasing in the order of A > B > C among the three stations in winter and contributing to decreased upstream sediment transport from Station A to Station C. Uncles et al. (2002) reported that long microtidal estuarine regimes can have extensive “intrinsic” SPM concentrations, and the storage mechanisms produce maximum turbidity areas in the upper reaches of numerous tidal estuaries. The long microtidal estuarine regimes are under limited low discharge situations and are left with substantial amounts of sediment materials influenced by tidal hydrodynamics that increase over the long term.

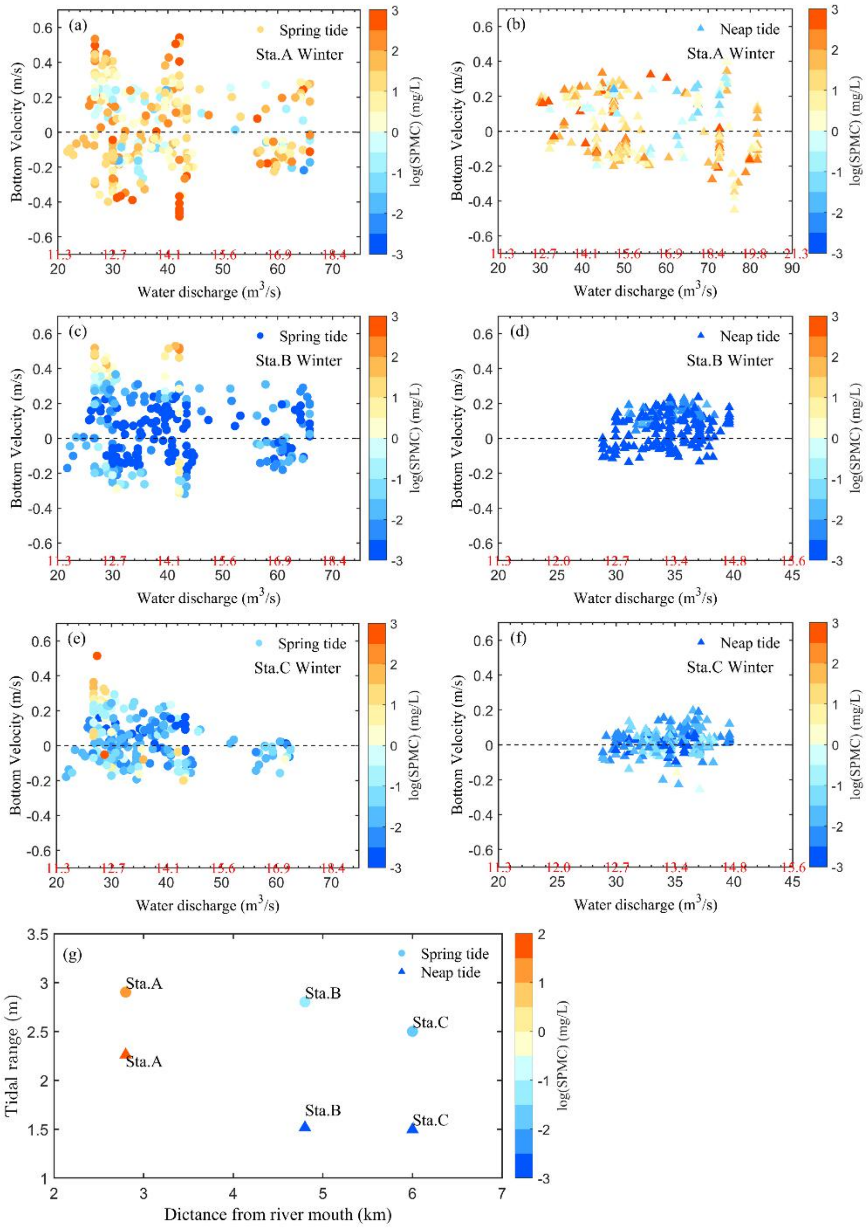

Fig. 10 Bottom tidal velocity *vs.* water discharge and SPMC for three stations during spring/neap tide period during winter and distribution of spring/neap tidal averaged bottom layer SPMC *vs*. tidal range at three stations during winter.

A comparison of the spring/neap tidal averaged bottom layer SPMC is shown in Fig 10. The higher SPMC at Station A is closely associated with the bed resuspension, while the lower SPMCs at Stations B and C indicate the weak resuspension process within either spring or neap tide (Fig. 10). The tidal range decreases with the distance from the river mouth (A > B > C). During both the spring and neap tide periods, the SPMC at Station A is higher than those at both Stations B and C. The SPMC magnitudes have the relationship A > B ≈ C. For the Otagawa floodway, considering sediment flux continuity, short-term sediment deposition occurs with the tidal pumping, most of the sediments are under the upstream transport and are deposited between Stations A and B during spring tide. On the other hand, during neap tide, most of the sediment undergoes local resuspension and settling.

The pattern of upstream transport is predominant in the lower and middle parts of the floodway during prolonged periods of low river runoff. Strong tidal asymmetry in velocity and duration can be dominant in driving sediment transport. From this work, short-term sediment deposition occurs along the area located between 2.8 km and 4.8 km from the mouth. However, the sediment load is exported to the near shore on a yearly to centennial scale (Brothers et al., 2008; Garel et al., 2009). More frequent low-discharge events enhance aggregation, settling, and trapping within the floodway.

4.3 Occurrence of convergence zone (CZ) in the tidal floodway

CZ location prediction is necessary in floodways and is of particular importance in order to improve regional sediment management. In the present work, based on the seasonal and spatial properties of the SPMC that were discussed in the previous sections, it was necessary to find the CZ between tidal and river forcings that occur along the floodway. The position of the depocenter along the floodway depends mainly on the tidal and river forcings, as already discussed in section 4.2. Under tidal control, most of sediment deposition occurs in the area between 2.8 km and 4.8 km from the mouth. To understand the relationship between the SPMC and river flow more fully, Fig. 11 depicts the SPMC as a function of the river discharge (in 20 m^3/s intervals) at Station A

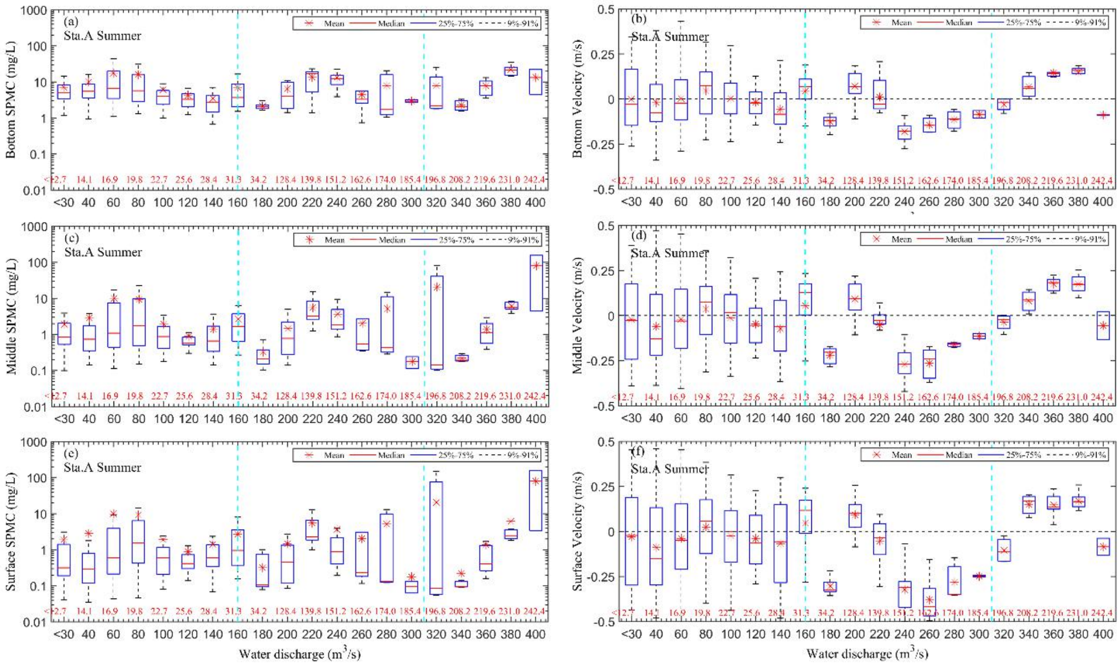

Fig. 11 Mean (red cross), median (red bars), 25–75th percentile (blue bars), and 9–91st

percentile (black bars) values of each layer-average SPMC (bottom, middle, and surface) in 20 m^3/s intervals of water discharge at Station A.

Determining the precise discharge threshold of CZ installation per station is challenging due to a large SPMC variability. Differences between the velocities during the periods of decreasing and increasing river flow are also notable in the floodway (Figs. 11b, 11d, and 11f). For discharge ($Q_{Yaguchi}$) less than 160 m^3/s (Q_{Gion} < 31 m^3/s), the small variations in the SPMC and velocities are associated with the highest potential for promoting CZ installation. Thus, the tidal pumping effect and river forcing converge around 2.8 km upstream from the river mouth. Discharge ($Q_{Yaguchi}$) greater than 160 m^3/s (Q_{Gion} > 31 m^3/s) can considerably promote CZ installation with dominant seaward currents, and large SPMC variation with one order of magnitude occurred in three layers. When discharge ($Q_{Yaguchi}$) greater than 310 m^3/s (Q_{Gion} > 191 m^3/s) seems to ensure complete CZ installation, significant variability from middle and surface layer SPMC is observable (blue bars varied from 0.1 to 100). Meanwhile, the SPMC is stable in the bottom layer. Within the bottom layer, the SPMC remains stable under tidal forcings, while in the middle and surface layers, the SPMCs show notable variations owing to the river forcings.

The effect of river discharge is assumed to be the primary factor in the occurrence of CZ. However, morphological changes (natural or anthropogenic) may also contribute to the CZ intensification (de Jonge et al., 2014), by amplifying the tidal asymmetry and hence enhancing the trapping of sediments. The existence and importance of these changes in the floodway could cause problems with the river flow in the foreseeable future, and it is necessary to investigate these issues further.

5. Conclusions

The relative effects of environmental forcings on the SPMC were evaluated on a seasonal scale by SSA, which is a powerful method for determining the contributions of environmental forcings on the SPMC. In summer, the ebb/flood velocities forcing (RC2) at Sta. A_R explained 9.6% of the variance, together with the contribution of the spring-neap tide oscillation (RC1, 81.9%). In winter at Sta. A_C, when the discharge was low and controlled by the Gion gates at upstream, the spring-neap tide oscillation (RC1) contributed 73.6% of the SPMC variance, together with the 19.5% of variance from the ebb/flood velocities (RC2). In contrast, at Stations B and C, most of the variance (up to 94.5%–96.9%) was contributed by the spring-neap tidal cycle. The detailed analysis based on the spring-neap tidal cycle with raw time-series data during summer and winter at Station A revealed the effects of ebb/flood currents. Spring tides matched the occurrences of higher SPMC and significant SPM upstream transport, whereas neap tides corresponded to times of lower SPMC and insignificant SPM transport. These characteristics are the results of higher tidal velocities during spring tides, which increase the availability of SPM within the brackish water column.

In the case of limited river runoff, the domain effects of oscillations related to the spring-neap tide cycle and flood-ebb cycle (reciprocating tidal velocity) on the SPMC variability along the Otagawa floodway were highlighted. Moreover, the role of discharge transport at less than 110 m^3/s (Q_{Gion} = 24 m^3/s) (winter and summer) demonstrated that tidal pumping has a domain effect on sediment shifting, while significant sediment seaward shifting results from flood events. Furthermore, a sort of "convergence" between tidal and river forcings seems to occur in the floodway. Upstream transport was observed with tidal pumping in most cases, while significant seaward transport corresponded to episodic flood events.

Although this study is a case-specific example of the Otagawa floodway, the presented results and discussion demonstrate the dynamics and mobility of SPM under tidal hydrodynamics in water discharge limited by artificial sluice gates. The results obtained in this study can be considered to contribute to increasing understanding of sediment dynamics in estuarine systems.

Acknowledgments

The author (CONG XIAO) gratefully acknowledges the financial support provided by the China Scholarship Council (CSC) for his Ph.D. studies at Hiroshima University. The authors acknowledge the students who participated in the observations and obtained valuable data for this work. This work was supported by JSPS KAKENHI grant number JP17H03313.

Reference

Al Sawaf, M.B., Kawanisi, K., Kagami, J., Bahreinimotlagh, M., Danial, M.M., 2017. Scaling characteristics of mountainous river flow fluctuations determined using a shallow-water acoustic tomography system. Physica A: Statistical Mechanics and its Applications 484, 11-20.

Baeye, M., Fettweis, M., Voulgaris, G., Van Lancker, V., 2011. Sediment mobility in response to tidal and wind-driven flows along the Belgian inner shelf, southern North Sea. Ocean Dynamics 61, 611-622.

Brothers, L., Belknap, D., Kelley, J., Janzen, C., 2008. Sediment transport and dispersion in a cool-temperate estuary and embayment, Saco River estuary, Maine, USA. Mar. Geol. 251, 183-194.

Burchard, H., Hetland, R.D., Schulz, E., Schuttelaars, H.M., 2011. Drivers of residual estuarine circulation in tidally energetic estuaries: Straight and irrotational channels with parabolic cross section. J. Phys. Oceanogr. 41, 548-570.

de Jonge, V.N., Schuttelaars, H.M., van Beusekom, J.E., Talke, S.A., de Swart, H.E., 2014. The influence of channel deepening on estuarine turbidity levels and dynamics, as exemplified by the Ems estuary. Estuar. Coast. Shelf Sci. 139, 46-59.

Duncker, J.J., Johnson, K.K., Sharpe, J.B., 2015. Bathymetric survey of Lake Calumet, Cook County, Illinois. US Geological Survey.

Ferreira, A.M., Martins, M., Vale, C., 2003. Influence of diffuse sources on levels and distribution of polychlorinated biphenyls in the Guadiana River estuary, Portugal. Mar. Chem. 83, 175-184.

French, J., Burningham, H., Benson, T., 2008. Tidal and meteorological forcing of suspended sediment flux in a muddy mesotidal estuary. Estuaries and Coasts 31, 843.

Garel, E., Pinto, L., Santos, A., Ferreira, Ó., 2009. Tidal and river discharge forcing upon water and sediment circulation at a rock-bound estuary (Guadiana estuary, Portugal). Estuar. Coast. Shelf Sci. 84, 269-281.

Ge, J., Zhou, Z., Yang, W., Ding, P., Chen, C., Wang, Z.B., Gu, J., 2018. Formation of Concentrated Benthic Suspension in a Time-Dependent Salt Wedge Estuary. Journal of Geophysical Research: Oceans 123, 8581-8607.

Geyer, W.R., MacCready, P., 2014. The estuarine circulation. Annual Review of Fluid Mechanics 46, 175-197.

Grabemann, I., Uncles, R., Krause, G., Stephens, J., 1997. Behaviour of turbidity maxima in the Tamar (UK) and Weser (FRG) estuaries. Estuar. Coast. Shelf Sci. 45, 235-246.

Jalón-Rojas, I., Schmidt, S., Sottolichio, A., 2016. Evaluation of spectral methods for high-frequency multiannual time series in coastal transitional waters: advantages of combined analyses. Limnol. Oceanogr. Methods 14, 381-396.

Kaneko, A., Zhu, X.-H., Radenac, M.-H., 1997. Diurnal variability and its quantification of subsurface sound scatterers in the western equatorial Pacific. Oceanographic Literature Review 44, 300-300.

Kawanisi, K., Bahrainimotlagh, M., Al Sawaf, M.B., Razaz, M., 2016. High-frequency streamflow acquisition and bed level/flow angle estimates in a mountainous river using shallow-water acoustic tomography. Hydrological Processes 30, 2247-2254.

Kawanisi, K., Razaz, M., Kaneko, A., Watanabe, S., 2010. Long-term measurement of stream flow and salinity in a tidal river by the use of the fluvial acoustic tomography system. Journal of Hydrology 380, 74-81.

Kawanisi, K., Tsutsui, T., Nakamura, S., Nisimaki, H., 2006. Influence of tidal range and river discharge on transport of suspended sediment in the Ohta flood-way. Journal of hydroscience and hydraulic engineering 24, 1-9.

Kawanisi, K., Yokayama, T., Razaz, M., Fukuoka, S., Abe, T., 2008a. Observations of Effect of Wind on Sediment Transport in Ohtagawa Estuary, Proceedings of Coastal Engineering, JSCE. Japan Society of Civil Engineers, pp. 386-390.

Kawanisi, K., Yokosi, S., 1997. Characteristics of suspended sediment and turbulence in a tidal boundary layer. Cont. Shelf Res. 17, 859-875.

Kawanisi, K., Yokoyama, T., Mizuno, M., Fukuoka, S., 2008b. Measurement of Suspende Sediment on Tidal Falt with an Acoustic Foppler Current Profiler. Proceedings of Hydraulic Engineering 52, 949-954.

Latosinski, F.G., Szupiany, R.N., García, C.M., Guerrero, M., Amsler, M.L., 2014. Estimation of concentration and load of suspended bed sediment in a large river by means of acoustic Doppler technology. Journal of Hydraulic Engineering 140, 04014023.

Moore, S., Le Coz, J., Hurther, D., Paquier, A., 2013. Using multi-frequency acoustic attenuation to monitor grain size and concentration of suspended sediment in rivers. The Journal of the Acoustical Society of America 133, 1959-1970.

Moura, M.G., Quaresma, V.S., Bastos, A.C., Veronez, P., 2011. Field observations of SPM using ADV, ADP, and OBS in a shallow estuarine system with low SPM concentration—Vitória Bay, SE Brazil. Ocean Dynamics 61, 273-283.

Murphy, S., Voulgaris, G., 2006. Identifying the role of tides, rainfall and seasonality in marsh sedimentation using long-term suspended sediment concentration data. Mar. Geol. 227, 31-50.

Razaz, M., 2010. Turbulence structures and transport processes of suspended sediment in the

Ōta diversion channel. PhD Thesis. Hiroshima University.

Razaz, M., Kawanisi, K., 2009. Long-Term Observations of Flow and Suspended Sediment in a Tidally-Dominated Estuary, Proceedings Of Coastal Dynamics 2009: Impacts of Human Activities on Dynamic Coastal Processes (With CD-ROM). World Scientific, pp. 1-11.

Razaz, M., Kawanisi, K., 2012. Tide-driven controls on maximum near-bed floc size in a partially-mixed estuary. Journal of Japan Society of Civil Engineers, Ser. B1 (Hydraulic Engineering) 68, I_7-I_12.

Razaz, M., Kawanisi, K., Nistor, I., 2015. Tide-driven controls on maximum near-bed floc size in a tidal estuary. Journal of Hydro-environment Research 9, 465-471.

Schoellhamer, D.H., 1996. Factors affecting suspended-solids concentrations in south San Francisco Bay, California. Journal of Geophysical Research: Oceans 101, 12087-12095.

Schoellhamer, D.H., 2001. Singular spectrum analysis for time series with missing data. Geophys. Res. Lett. 28, 3187-3190.

Schoellhamer, D.H., 2002. Variability of suspended-sediment concentration at tidal to annual time scales in San Francisco Bay, USA. Cont. Shelf Res. 22, 1857-1866.

Scully, M.E., Friedrichs, C.T., 2003. The influence of asymmetries in overlying stratification on near-bed turbulence and sediment suspension in a partially mixed estuary. Ocean Dynamics 53, 208-219.

Shi, J.Z., 2010. Tidal resuspension and transport processes of fine sediment within the river plume in the partially-mixed Changjiang River estuary, China: a personal perspective. Geomorphology 121, 133-151.

Thorne, P.D., Hanes, D.M., 2002. A review of acoustic measurement of small-scale sediment processes. Cont. Shelf Res. 22, 603-632.

Uncles, R., Stephens, J., Smith, R., 2002. The dependence of estuarine turbidity on tidal intrusion length, tidal range and residence time. Cont. Shelf Res. 22, 1835-1856.

Van Leussen, W., Dronkers, J., 1988. Physical processes in estuaries: An introduction, Physical processes in estuaries. Springer, pp. 1-18.

Vautard, R., Yiou, P., Ghil, M., 1992. Singular-spectrum analysis: A toolkit for short, noisy chaotic signals. Physica D: Nonlinear Phenomena 58, 95-126.

Voulgaris, G., Meyers, S.T., 2004. Temporal variability of hydrodynamics, sediment concentration and sediment settling velocity in a tidal creek. Cont. Shelf Res. 24, 1659-1683.

Wang, N., Chen, K., Lu, P., Chen, Y., Zhang, J., Wang, Y., 2019. Impact of a water–sediment regulation scheme on the hydrodynamics and sediment conditions in the Sheyang Estuary. Estuar. Coast. Shelf Sci. 218, 349-358.

Zhu, X.-H., Takasugi, Y., Nagao, M., Hashimoto, E., 2000. Diurnal cycle of sound scatterers and measurements of turbidity using ADCP in Beppu Bay. J. Oceanogr. 56, 559-565.

Appendix: Supplemental Data

A.1: Grain size variations along the Otagawa floodway

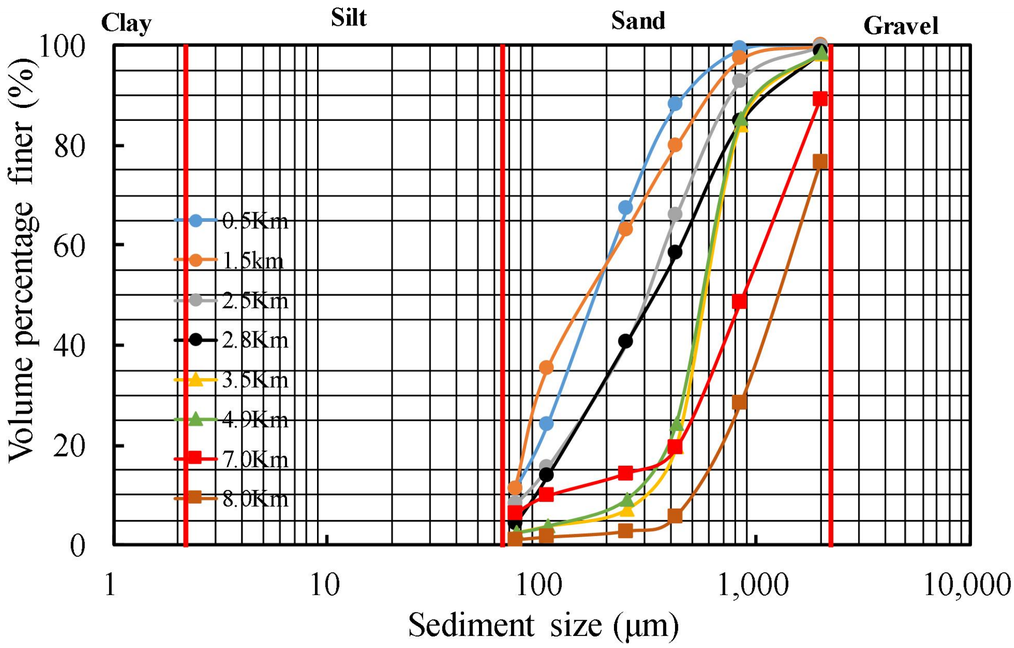

Fig. A.1 Grain size variations along the Otagawa floodway.

A.2: Relationships of the RCs to the temporal changes of the variables at Sta. A_R summer, Sta. A_C winter, Station B, and Station C.

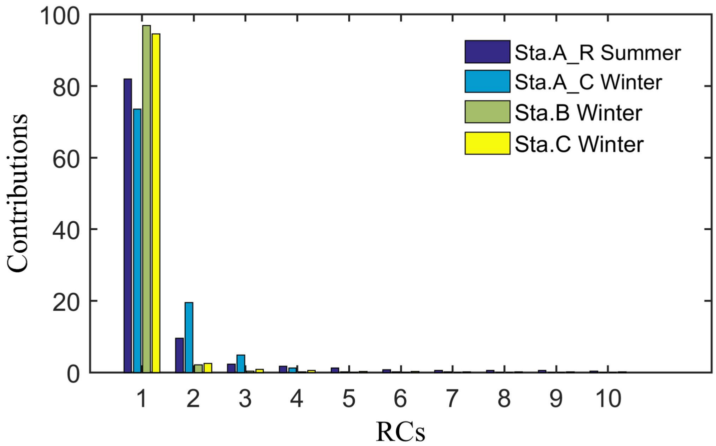

Fig. A.2 (a) RC contributions to four SPMC time series: during summer at Sta. A_R from July 29 to August 16, 2007; during winter at Sta. A_C from January 6 to 26, 2008; during winter at Sta. B from December 22, 2007 to January 16, 2008; during winter at Sta. C from December

27, 2007 to January 10, 2008.

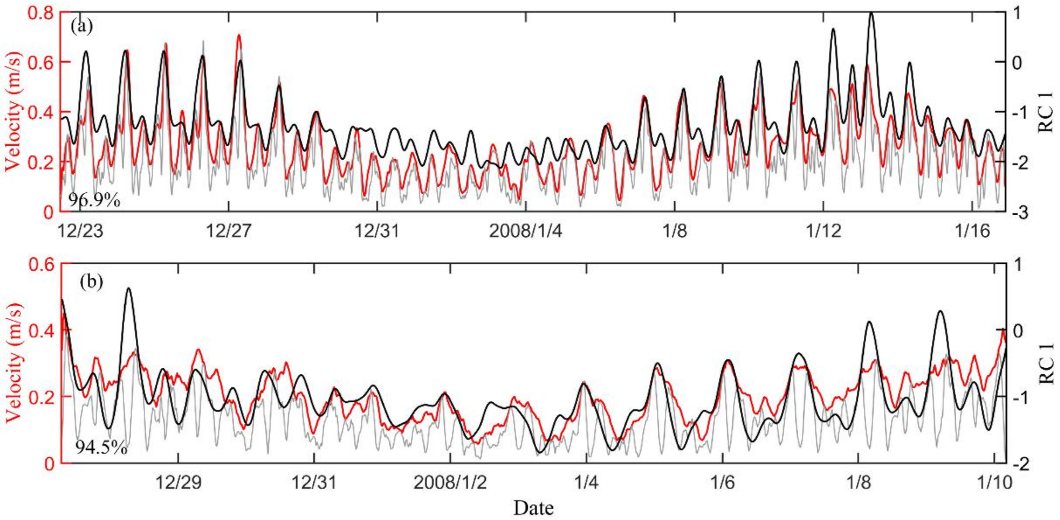

Fig. A.2 (b) Comparisons of the RCs to the temporal changes in the variables at Stations B and C, including: (a) at Station B RC1 vs. velocity (the red line represents the envelope of the velocity and the gray line represents the original velocity), (b) at Station C RC1 vs. velocity (the red line represents the envelope of the velocity and the gray line represents the original velocity). The contribution of each RC to the total SPMC variability is written in the bottom left corner, where the first mode accounts for 96.9% and 94.5% of the SPMC variance at Stations B and C, respectively.

A.3: Temporal variations of the velocity and SPMC profiles at Stations B and C.

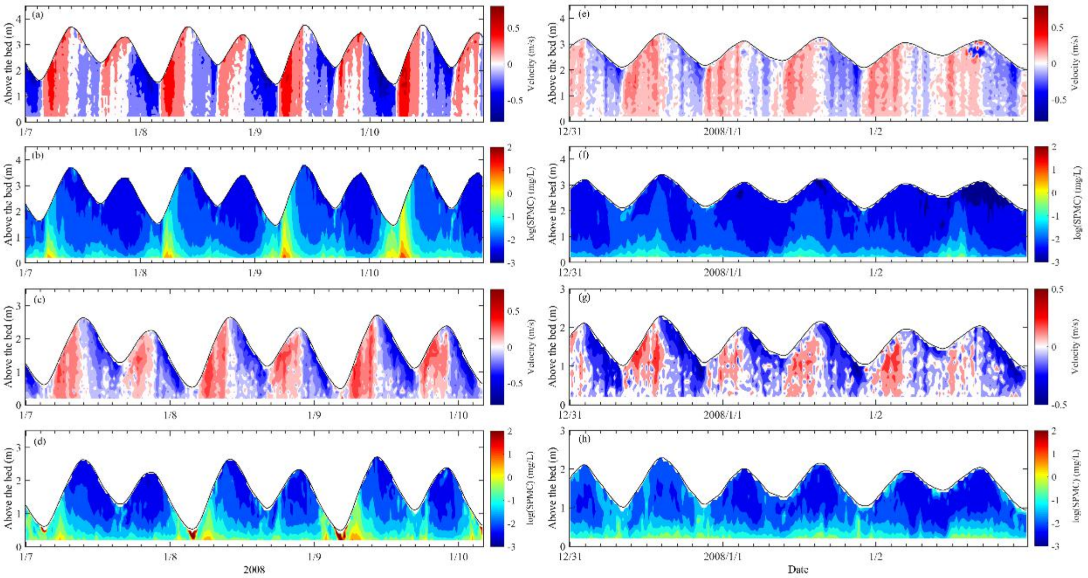

Fig. A.3 Temporal variations of the velocity profile (positive indicates flood, upstream) and SPMC, including (a) velocity and (b) SPMC at Station B during spring tide, (c) velocity and (d) SPMC at Station C during spring tide, (e) velocity and (f) SPMC at Station B during neap tide, and (g) velocity and (h) SPMC at Station C during neap tide.

A.4: SPMC cumulative flux at Stations A, B, and C

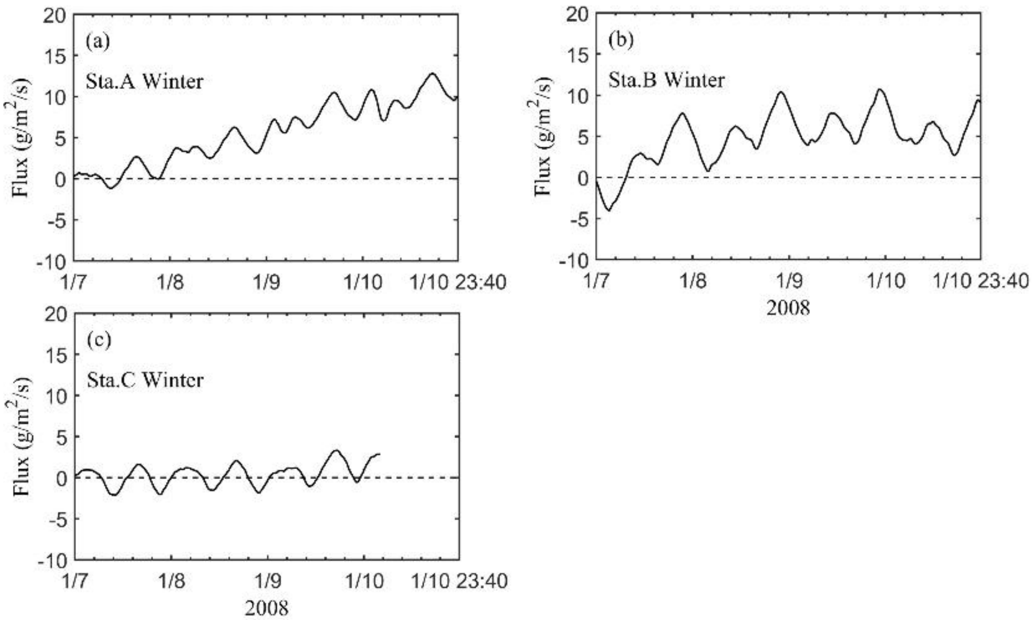

Fig. A.4 Comparison of SPMC cumulative flux at Stations A, B, and C during January 7–10, 2008.